Int. J. Appl. Math. Comput. Sci., 2023, Vol. 33, No. 4, 521–535
DOI: 10.34768/amcs-2023-0038

ROBUST FLAT FILTERING CONTROL OF A TWO DEGREES OF FREEDOM HELICOPTER SUBJECT TO TAIL ROTOR DISTURBANCES

VICTOR-GABRIEL SÁNCHEZ-MEZA [a], YAIR LOZANO-HERNÁNDEZ [b], OCTAVIO GUTIÉRREZ-FRÍAS [a], NORMA LOZADA-CASTILLO [a], ALBERTO LUVIANO-JUÁREZ [a,*]

[a] Interdisciplinary Professional Unit of Engineering and Advanced Technologies (UPIITA)
National Polytechnic Institute
Av. IPN 2580 Col. Barrio La Laguna Ticomán, CP 07340, Mexico City, Mexico
e-mail: vsanchezm1301@alumno.ipn.mx,
{ogutierrezf,nlozadac,aluvianoj}@ipn.mx

[b] Interdisciplinary Professional Unit of Engineering, Campus Hidalgo (UPIIH)
National Polytechnic Institute
Carretera Pachuca-Actopan Kilómetro 1+500, San Agustín Tlaxiaca, 42162, Hidalgo, Mexico
e-mail: ylozanoh@ipn.mx

This article deals with modelling and a flatness-based robust trajectory tracking scheme for a two degrees of freedom helicopter, which is subject to four types of tail rotor disturbances to validate the control scheme robustness. A mathematical model of the system, its differential flatness and a differential parametrization are obtained. The flat filtering control is designed for the system control with a partially known model, assuming the non-modelled dynamics and the external disturbances (specially the tail rotor ones) to be rejected by means of an extended state model (ultra-local model). Numerical and experimental assessments are carried out on a characterized prototype whose yaw angle (ψ), given by the z axis, is in free form, while the pitch angle (θ), which results from rotation about the y axis, is mechanically restricted. The proposed controller performance is tested through a set of experiments in trajectory tracking tasks with different disturbances in the tail rotor, showing robust behaviour for the different disturbances. Besides, a comparison study against a widely used controller of LQR type is carried out, in which the proposed controller achieves better results, as illustrated by a performance index.

Keywords: flat filtering control, generalized proportional integral control, non-linear systems, tail rotor disturbance, two degrees of freedom helicopter.

1. Introduction

The research in the field of rotary wing unmanned aerial vehicles (UAVs) has attracted attention from the research and industry communities due to a variety of traditional and emerging applications, from the development of the Internet of things and new generation wireless communication systems, to surveillance schemes, to flight control development devices and theoretical contributions among others (Zeng *et al.*, 2019; Zhan and Huang, 2020; Ferdaus *et al.*, 2020; Ordaz *et al.*, 2023; Pizetta *et al.*, 2016; Ross *et al.*, 2022).

*Corresponding author

Helicopters are among rotary wing UAVs (Leishman, 2007; Kantue and Pedro, 2022), whose main features are the capacity of rotation on its own axis, levitation, take off and landing performed vertically, and that they can move in their three axes of translation while in the air, etc. In addition, there are different configurations that range from containing one rotor or more (Nonami *et al.*, 2010); some of them have even been modified to provide hybrid configurations (Tavoosi, 2021).

Due to the non-linearities and the coupling in the dynamics between the performances of both rotors, the helicopter has been a subject of research to improve its stability and to compensate disturbances of internal and external nature (Zhu and Huo, 2013; Wang *et al.*, 2020), which involve a constant effort to improve the robustness and performance of these systems (Budiyono and Wibowo, 2007; He *et al.*, 2021; Raffo *et al.*, 2015; Rysdyk and Calise, 1999; Kasac *et al.*, 2019). The necessity of validating control schemes under defined conditions has motivated the development of different experimental test benches and prototypes, most of which being focused on specific applications (Bortoff, 1999; Garcia and Valavanis, 2008; Vitzilaios and Tsourveloudis, 2009).

One of the most popular platforms used to recreate part of the dynamics is the two-degrees-of-freedom helicopter (henceforth TDFH), which recreates a subset of the helicopter's dynamic behaviour on its pitch (θ) and yaw (ψ) rotations (Ahmed *et al.*, 2010). Its orientation is actuated by the joint work of two rotors with their respective propellers and both positioned at the ends of a rigid shaft attached to a rotating base that allows it to rotate about the y and z axes (Nilsen, 2017).

However, there is a reduced number of commercial TDFH prototypes with an open architecture that take account of the presence of aerodynamic effects that usually arise (Lynn *et al.*, 1970; Tanner and Geering, 2003) and/or that allow modifications to its structure to assess various control algorithms (Lozano-Hernandez and Gutierrez-Frias, 2016; Kutay *et al.*, 2005; Liu, 2022). Furthermore, in helicopters, the tail rotor (hereinafter TR) is affected on a larger scale by disturbances, causing flight stability problems (Nilsen, 2017; Velagic and Osmic, 2010). For this reason, prototypes that allow inducing perturbations in the TR are required to validate stability tests.

In addition to the above, in the work of Schäferlein *et al.* (2018), rotor-fuselage interactions often face problems in fast-forward flight caused by strong tail interactions, the so-called "tail shake phenomenon". On the other hand, Lynn *et al.* (1970) carry out the study of aerodynamic interferences in the TR that are generated by the main rotor (hereinafter MR), while Sánchez-Meza *et al.* (2020) simulate generalized proportional integral (GPI) control of the TDFH in the presence of disturbances in the TR. Additionally, Tang *et al.* (2019) show that the force varies in a quadratic relationship between the pitch of the propellers and the speed of rotation, thus highlighting the importance of rejecting this type of disturbance.

Regarding the implementation of control algorithms, Kumar *et al.* (2016) present a comparison of particle swarm optimization (PSO) methods against adaptive particle swarm optimization (APSO), to set the Q and R matrices necessary to implement the LQR controller, whose control task is to follow a sinusoidal trajectory in the pitch angle and to stabilize the yaw angle before a step. In addition, Butt and Aschemann (2015) design multi-variable integral sliding mode control to track the desired trajectories for both pitch and yaw angles. Discrete-time extended Kalman filters (EKFs) are also used and combined with a non-linear control law for the estimation of non-measurable states. Moreover, in the work of Rojas-Cubides *et al.* (2019), a sliding mode control scheme is proposed for the TDFH using generalized proportional integral type observers to estimate and cancel perturbations caused by non-modelled dynamics and external perturbations.

A special case of active disturbance rejection which is free of state observers (Ramírez-Neria *et al.*, 2021), but with an equivalent response to that of an extended state observer-based control (Sira-Ramírez *et al.*, 2019) is the flat filtering control. This is based on the principle of controlling an extended state model (here termed as the ultra-local model (Fliess and Join, 2013; Sira-Ramírez *et al.*, 2017)), which lumps the uncertainties and external disturbances into a generalized disturbance input, which is to be rejected by generalized proportional integral control actions (such as GPI control (Fliess *et al.*, 2002)). The control input synthesis includes an implicit control structure (compensation network) which leads to a filtering realization of the control that is capable of rejecting a wide variety of disturbances for differentially flat systems. Since this scheme avoids using state observers, some aspects such as sensitivity to measurement noise are improved in the closed loop control while achieving the robustness aspects of the extended state disturbance mitigation.

This article intends to design a control scheme based on flat filtering that allows to compensate for unmodeled dynamics and the attenuation of time-varying disturbances, in particular the periodic ones, which can be considered as part of the flight transition stage of a hybrid aircraft. For this, a model of a two degrees of freedom helicopter with a mechanism to generate disturbances in the tail rotor is presented. This model is used to analyse the performance of control schemes subjected to disturbances in the tail rotor, which could be considered as disturbances due to wind gusts, structural failures, aerodynamic effects, and hybrid flight mode transitions (Tavoosi, 2021), among others. Likewise, the mathematical model that takes account of the disturbances in the tail rotor and the non-linear characteristics was developed. The flatness property of the system and the synthesis of a flat filtering control scheme designed to track, compensate and attenuate the induced disturbances are also presented.

Besides, in this article, the stability test of the proposed control system is given in terms of Lyapunov's second method as well as some Bode tests to illustrate the disturbance attenuation, in contrast to the former flat filtering contributions whose stability test is purely based on linearly dominant dynamics, leading to a BIBO behavior. Likewise, the control scheme was tested experimentally and the results prove the robustness of the flat filtering scheme against a set of different tail rotor perturbations, while achieving competitive tracking results on rest-to-rest trajectory tracking tasks.

The organization of this work is as follows. In Section 2, the dynamic model of the TDFH is developed, taking into account the variations in the tail rotor; also, the differential flatness property of the system is obtained. Section 3 presents the problem formulation and the flat filtering control design. Section 4 shows the experimental test bed and the results of the control test set under different disturbance inputs, as well as a comparison with a popular control scheme for this class of systems. Finally, some final considerations of the presented work are given.

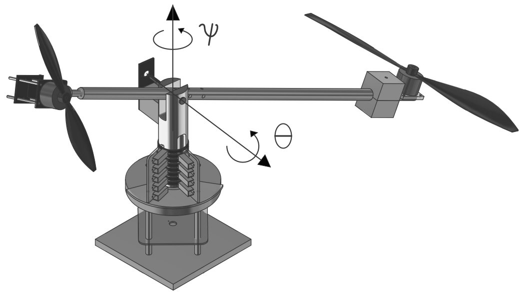

(a) TDFH scheme.

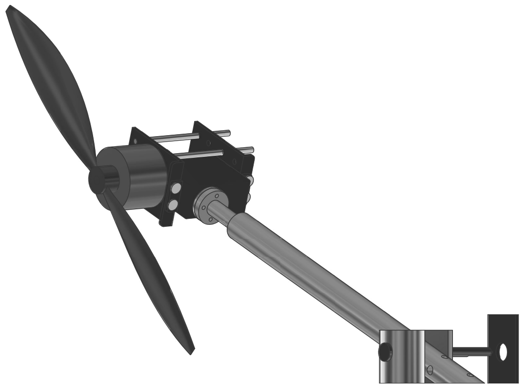

(b) coupling for the generation of disturbances in the TR.

Fig. 1. Proposed design.

2. Mathematical modelling

The TDFH recreates a behaviour subset of the conventional helicopter's actual dynamics on the pitch and yaw rotations. These rotations represent the two degrees of freedom of its centre of mass. In particular, the proposed TDFH consists of a main rotor and a tail rotor attached to a rotational axis for pitch (see Fig. 1(a)).

The TDFH model used in this work was inspired by the prototypes presented by Ahmed *et al*. (2010) Lynn *et al*. (1970) or Tanner and Geering (2003), but with some modifications in the structure to integrate rotating rings in the yaw rotation, a mechanism to generate perturbations in the TR rotation and the incorporation of a mass to generate a displacement of the centre of gravity. This model is illustrated in Fig. 1(a), while the electromechanical system dedicated to generating disturbances in the tail rotor is shown in Fig. 1(b); it is important to indicate that this mechanism does not increase the degrees of freedom, but it only alters the incidence of action of the TR on the system. The disturbances generated in the TR can be considered as effects of transition stages of hybrid systems, aerodynamic phenomena such as wind gusts or the flutter effect, structural damages, among others. This allows an analysis of the system behaviour, generating different types of disturbances in a controlled way that can resemble the required phenomena.

Analogously, the free body diagrams that indicate the parameters and variables of interest of the TDFH are shown in Fig. 2, where the angles of rotation about the 'yaw' and 'pitch' axes are defined by ψ and θ, respectively, the force of gravity is represented by F_g, while the thrust forces exerted by the rotors TR and MR are denoted by F_y and F_p, respectively; the distance of the centre of mass from the axis of rotation of the pitch and about the X coordinate is denoted by L_{cm}; the distances from the TR and MR to the pitch axis are given by r_y and r_p, respectively. Also, the angle of incidence of the TR thrust force is ϕ and its axis of rotation projects through the X axis. Finally, the inertial coordinate frame is given by $O_0X_0Y_0Z_0$.

In this work, the calculation of the dynamic model of the THDF was based on the methodology reported by Kumar *et al*. (2016). The kinematics of the TDFH is obtained starting from Fig. 2. Thus, the homogeneous matrix H that represents the translation and rotation of the TDFH with respect to the reference frame (centre of gravity) is described by

$$H = \begin{bmatrix} c_\psi c_\theta & s_\psi & -c_\psi s_\theta & L_{cm} c_\psi c_\theta \\ -s_\psi c_\theta & c_\psi & s_\psi s_\theta & -L_{cm} s_\psi c_\theta \\ s_\theta & 0 & c_\theta & L_{cm} s_\theta \\ 0 & 0 & 0 & 1 \end{bmatrix}, \tag{1}$$

where H is a function of the rotation variables ψ and θ, and the following notation is adopted: for an argument α, $s_\alpha := \sin(\alpha)$, $c_\alpha := \cos(\alpha)$ (this notation will be used in the rest of the document). The position of the centre of mass on the axes X, Y and Z is expressed by

$$\begin{aligned} X &= L_{cm} c_\psi c_\theta, \\ Y &= -L_{cm} s_\psi c_\theta, \\ Z &= L_{cm} s_\theta. \end{aligned} \tag{2}$$

The dynamic model of the system is obtained from the Euler–Lagrange approach (Siciliano *et al*., 2010):

$$\tau = \frac{\mathrm{d}}{\mathrm{d}t}\frac{\partial \mathcal{L}}{\partial \dot{q}} - \frac{\partial \mathcal{L}}{\partial q} + B\dot{q}, \tag{3}$$

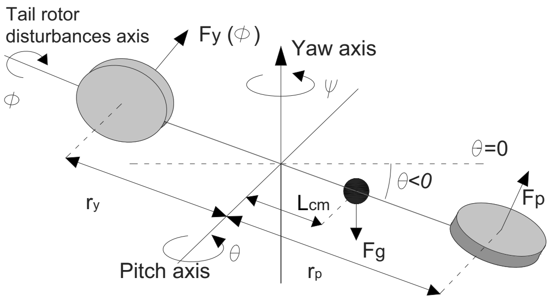

(a) TDFH variables and parameters.

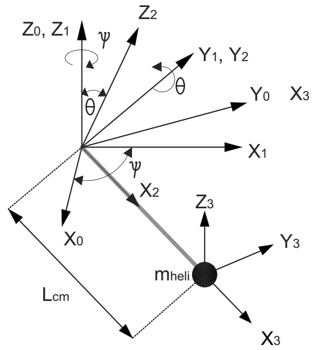

(b) free-body diagram of the TDFH.

Fig. 2. Diagrams of the TDFH.

where $\mathcal{L} = T - U$ is the Lagrangian with T and U denoting the kinetic and potential energies, respectively, τ is the force associated to the generalized coordinates $q = \begin{bmatrix}\theta & \psi\end{bmatrix}^\intercal$, and B is the viscous friction coefficient matrix.

Subsequently, the kinetic and potential energies are defined by

$$\begin{aligned} T &= T_{r\theta} + T_{r\psi} + T_t, \\ U &= m_h L_{cm} \bar{g} s_\theta, \end{aligned} \tag{4}$$

where the mobile mass of the TDFH is denoted by m_h, the gravity constant is $\bar{g}$; the kinetic energies of rotation on the components ψ and θ are $T_{r\theta}$ and $T_{r\psi}$ respectively; on the other hand, the kinetic energy of translation is represented by T_t. The energies are calculated as

$$\begin{aligned} T_{r\theta} &= \frac{1}{2} J_\theta \dot{\theta}^2, \\ T_{r\psi} &= \frac{1}{2} J_\psi \dot{\psi}^2, \\ T_t &= \frac{1}{2} m_h \left(V_x^2 + V_y^2 + V_z^2\right), \end{aligned} \tag{5}$$

where J_θ is the moment of inertia about the coordinate θ; analogously, J_ψ is the moment of inertia about ψ. In addition, the speeds on the axes X, Y and Z are obtained from the time derivative of (2). In this way, the rotational kinetic energy is expressed in the form

$$T_t = \frac{1}{2} m_h L_{cm}^2 \left(\dot{\theta}^2 + (\dot{\psi} c_\theta)^2\right). \tag{6}$$

Finally, the resulting kinetic energy is

$$T = \frac{1}{2} J_\theta \dot{\theta}^2 + \frac{1}{2} J_\psi \dot{\psi}^2 + \frac{1}{2} m_h L_{cm}^2 \left(\dot{\theta}^2 + (\dot{\psi} c_\theta)^2\right). \tag{7}$$

The Lagrangian is calculated by

$$\begin{aligned} \mathcal{L} = {} & \frac{1}{2} J_\theta \dot{\theta}^2 + \frac{1}{2} J_\psi \dot{\psi}^2 + \frac{1}{2} m_h L_{cm}^2 \left(\dot{\theta}^2 + (\dot{\psi} c_\theta)^2\right) \\ & - m_h \bar{g} s_\theta L_{cm}. \end{aligned} \tag{8}$$

Additionally, the generalized forces $\tau = \begin{bmatrix}\tau_\theta & \tau_\psi\end{bmatrix}^\intercal$, undergo modifications to the torques applied to the TDFH with respect to Kumar *et al.* (2016), derived from disturbances in the angle ϕ (see Fig. 1(b)) which directly affect the TR push force. Thus, the pairs are defined by

$$\begin{bmatrix}\tau_\theta \\ \tau_\psi\end{bmatrix} = \begin{bmatrix} k_{\theta\theta} & k_{\psi\psi} s_\phi + k_{\theta\psi} c_\phi \\ k_{\psi\theta} & k_{\psi\psi} c_\phi + k_{\theta\psi} s_\phi \end{bmatrix} \begin{bmatrix} U_\theta \\ U_\psi \end{bmatrix} - \begin{bmatrix} B_\theta \dot{\theta} \\ B_\psi \dot{\psi} \end{bmatrix}, \tag{9}$$

where τ_θ and τ_ψ are the torques applied to each axis of rotation generated by the ratio of the control actions defined as U_θ and U_ψ (depending on the pulse width modulation technique, PWM) and the thrust force constants k_{ij} [Nm/% pwm], where i establishes the i-th rotor impinging on the j-th axis due to the direct thrust force of the rotor and by the propeller torque.

Substituting (8) and (9) in (3), the following dynamic equations are obtained:

$$\begin{aligned} & \begin{bmatrix} J_\theta + m_h L_{cm}^2 & 0 \\ 0 & J_\psi + m_h (c_\theta L_{cm})^2 \end{bmatrix} \begin{bmatrix} \ddot{\theta} \\ \ddot{\psi} \end{bmatrix} \\ & + m_h L_{cm}^2 s_\theta c_\theta \begin{bmatrix} 0 & \dot{\psi} \\ -\dot{\psi} & -\dot{\theta} \end{bmatrix} \begin{bmatrix} \dot{\theta} \\ \dot{\psi} \end{bmatrix} + \begin{bmatrix} B_\theta & 0 \\ 0 & B_\psi \end{bmatrix} \begin{bmatrix} \dot{\theta} \\ \dot{\psi} \end{bmatrix} \\ & + \begin{bmatrix} m_h \bar{g} L_{cm} c_\theta \\ 0 \end{bmatrix} = \begin{bmatrix} k_{\theta\theta} & k_{\psi\psi} s_\phi + k_{\theta\psi} c_\phi \\ k_{\psi\theta} & k_{\psi\psi} c_\phi + k_{\theta\psi} s_\phi \end{bmatrix} \begin{bmatrix} U_\theta \\ U_\psi \end{bmatrix}. \end{aligned} \tag{10}$$

Let us define $u := \begin{bmatrix}U_\theta & U_\psi\end{bmatrix}^\intercal$. Using the generalized coordinates, (10) can be rewritten as

$$D(q)\ddot{q} + C(q, \dot{q})\dot{q} + B\dot{q} + g(q) = Ku, \tag{11}$$

where $D(q)$ is the inertia matrix, $C(q, \dot{q})$ stands for the Coriolis matrix, B is the viscous friction matrix, $g(q)$ denotes the gravity vector, K represents the control gain matrix including the disturbance term ϕ, due to the tail rotor disturbances, which is assumed piecewise constant, and u is the control vector.

2.1. Differential flatness of the system. Consider the disturbance-free system (that is, $\phi = 0$). Then the gain matrix becomes

$$K = \begin{bmatrix} k_{\theta\theta} & k_{\theta\psi} \\ k_{\psi\theta} & k_{\psi\psi} \end{bmatrix}. \tag{12}$$

If $d_k := \det(K) = k_{\theta\theta}k_{\psi\psi} - k_{\theta\psi}k_{\psi\theta} \neq 0$, the system is differentially flat (Fliess *et al.*, 1995), where each variable of the system can be expressed in terms of the flat outputs $q_1 := \theta$, $q_2 := \psi$, their finite time derivatives, and their algebraic combination as represented in the following differential parametrization:

$$\begin{aligned}
\dot{\theta} &= \dot{q}_1, \\
\dot{\psi} &= \dot{q}_2, \\
U_\theta &= \frac{1}{d_k}\left[k_{\psi\psi}(J_\theta + m_h L_{cm}^2)\ddot{q}_1\right. \\
&\quad - k_{\theta\psi}(m_h(c_{q_1}L_{cm})^2 + J_\psi)\ddot{q}_2 \\
&\quad + m_h L_{cm}^2 s_{q_1} c_{q_1}(k_{\psi\psi}\dot{q}_2^2 + k_{\theta\psi}\dot{q}_1\dot{q}_2) \\
&\quad + k_{\psi\psi}B_\theta\dot{q}_1 - k_{\theta\psi}\dot{q}_2 \\
&\quad \left. + k_{\psi\psi}m_h\bar{g}L_{cm}c_{q_1}\right], \\
U_\psi &= \frac{1}{d_k}\left[-k_{\psi\theta}(J_\theta + m_h L_{cm}^2)\ddot{q}_1\right. \\
&\quad + k_{\theta\theta}(m_h(c_{q_1}L_{cm})^2 + J_\psi)\ddot{q}_2 \\
&\quad + m_h L_{cm}^2 s_{q_1} c_{q_1}(-k_{\psi\theta}\dot{q}_2^2 - 2k_{\theta\theta}\dot{q}_1\dot{q}_2) \\
&\quad - k_{\psi\theta}B_\theta\dot{q}_1 + k_{\theta\theta}B_\psi\dot{q}_2 \\
&\quad \left. - k_{\psi\theta}m_h\bar{g}L_{cm}c_{q_1}\right].
\end{aligned} \tag{13}$$

It is clear that the flat outputs coincide with the generalized coordinates of the system q. Moreover, it should be noted that the invertibility of the matrix K depends on the system parameters and a set of admissible values of ϕ (obtained from the calculation of the determinant of K). In this case, the parameters are given in Table 1, for which the range $-1.808\,\mathrm{rad} < \phi < 1.333\,\mathrm{rad}$ ensures the invertibility of K.

3. Control design

System (10) can be rewritten as

$$\begin{aligned}
\ddot{q} &= D^{-1}(q)\left[Ku + g(q)\right] \\
&\quad - D^{-1}(q)\left[C(q,\dot{q})\dot{q} + B\dot{q}\right],
\end{aligned} \tag{14}$$

Let us lump the dynamics of the viscous friction and Coriolis as well as possible arising additive external disturbances of uniformly bounded nature (not explicitly considered in the original model and represented by the variable $\eta(t) \in \mathbb{R}^2$) into a generalized disturbance input denoted as $\xi(t, q, \dot{q})$. That is,

$$\xi = -D^{-1}(q)\left[C(q,\dot{q})\dot{q} + B\dot{q} + \eta(t)\right]. \tag{15}$$

Furthermore, the effect of gravity $g(q)$ does not need to be considered as part of the disturbances, since it is a known and limited phenomenon depending on measurable variables in which $g(q)$ can be directly compensated by the feedforward control action such as the one carried out in traditional multivariable PD with gravity compensation control actions for robotic systems (Spong *et al.*, 2006). Also, substituting the generalized disturbance into the system, the following simplified system is obtained:

$$\ddot{q} = D^{-1}(q)\left[Ku + g(q)\right] + \xi(t, q, \dot{q}). \tag{16}$$

Taking advantage of the invertibility property of both $D(q)$ and K, and the bounds of the inertia matrix property (Spong *et al.*, 2006), without loss of generality the following auxiliary input can be defined:

$$v = D^{-1}(q)\left[Ku + g(q)\right]. \tag{17}$$

Using (17), the following perturbed system is obtained:

$$\ddot{q} = v + \xi(t, q, \dot{q}). \tag{18}$$

From the nature of the generalized disturbance inputs $\xi(t, q, \dot{q})$, it can be assumed that $\xi(t, q, \dot{q})$ is ultimately uniformly bounded with some finite bounded time derivatives.

3.1. Problem formulation. Consider the simplified representation of a disturbed TDFH system (18). It is desired to track a reference trajectory denoted by q^* through a robust output feedback control, despite the disturbance dynamics of external and internal nature lumped as a generalized function ξ.

3.2. Flat filtering control (FFC). The flatness property of the system along with the nature of the generalized disturbance input allow to implement an active disturbance rejection based control approach (see the work of Han (2009), Fareh *et al.* (2021), Ahi and Haeri (2018) or Madoński and Herman (2015) for a comprehensive review of the control approach and the use of extended state observers in disturbance estimation tasks) to compensate the disturbance input for a further application of a linear control on an integrator chain-like system. A classic relation between flatness-based disturbance rejection approaches involving extended state observers (classic active disturbance rejection) or flat filters (implicit disturbance estimation and cancellation through integral control actions) can be found in the work of Sira-Ramírez (2018). Among the considered pioneering contributions, the most recently introduced one consists of idealized exact compensation actions of a family of polynomials (algebraic phenomenological analysis), which contrasts with the presented stability analysis, which is a contribution of this study and consists in applying the Lyapunov second method for the approximated disturbance compensation of the closed-loop error dynamics. In this manuscript the proposal is based on a flat filtering controller (hereinafter FFC) to be described as follows.

Consider the sub-index i as the i-th component of (18). Let us define the output tracking error as $e_{qi} := q_i(t) - q_i^*(t)$, $i = 1, 2$. From (18), the feedforward control input for the unperturbed system is computed as $v_i^* = \ddot{q}_i^*$ (Sira-Ramírez *et al.*, 2017). Then, the difference between the control v_i and the feedforward input (typically known as the feedback part of the control) is defined as

$$e_{vi} := v_i(t) - v_i^*(t). \tag{19}$$

Then the tracking error dynamics is governed by the following equation:

$$\ddot{e}_{qi} = e_{vi} + \xi_i. \tag{20}$$

The generalized disturbance input $\xi_i(t)$ is locally modelled by means of the following extended state approximation (ultra-local model (Fliess and Join, 2013; Pereira das Neves and Augusto Angélico, 2022)):

$$\begin{aligned} \ddot{e}_{qi} &= e_{vi} + \rho_{1i}, \\ \dot{\rho}_{ji} &= \rho_{(j+1)i}, \quad j = 1, 2, \dots, m-1, \\ \dot{\rho}_{mi} &= 0. \end{aligned} \tag{21}$$

In order to avoid an asymptotic observer for $\dot{e}_q$, the following integral re-constructor is proposed

$$\hat{\dot{e}}_{qi} = \int_0^t e_{vi}(\tau)\,\mathrm{d}\tau. \tag{22}$$

For the unperturbed case, the relation between $\dot{e}_{qi}$ and $\hat{\dot{e}}_{qi}$ is $\dot{e}_{qi}(t) = \hat{\dot{e}}_{qi}(t) + \hat{\dot{e}}_{qi}(0)$. However, this relation is affected by the external disturbance ξ_i. To correct that effect, some iterative integral compensations of the output tracking error are given (Fliess *et al.*, 2002; Ramírez-Neria *et al.*, 2014). Taking the ultra-local model representation (21), the following GPI control is proposed:

$$\begin{aligned} e_{vi} = &-k_{(m+2)i}(\int e_{vi}) - k_{(m+1)i}e_{qi} \\ &- k_{(m)i}(\int e_{qi}) - k_{(m-1)i}(\int^{(2)} e_{qi}) \\ &- \dots - k_{(0)i}(\int^{(m+1)} e_{qi}), \end{aligned} \tag{23}$$

where the notation $\int^{(n)} f$ denotes the n-times iterated integral

$$\int^{(n)} f = \int_0^t \int_0^{\tau_1} \cdots \int_0^{\tau_{n-1}} f(\tau_{n-1})\,\mathrm{d}\tau_n \cdots \mathrm{d}\tau_1. \tag{24}$$

The disturbance approximation by the ultra-local model leads to the following relation:

$$\xi(t, q, \dot{q})_i = a^{\mathsf{T}} \kappa(t) + \tilde{\xi}_i, \tag{25}$$

where $a \in \mathbb{R}^m$ is a vector formed by a set of constant parameters such that the disturbance approximation is improved (Sira-Ramírez *et al.*, 2017; Ramírez-Neria *et al.*, 2016). From the family of time polynomial approximations, $\kappa = \begin{bmatrix} 1 & t & \cdots & t^{m-1} \end{bmatrix}^{\mathsf{T}}$. The differential form of last approximation is [1]

$$\begin{aligned} a^{\mathsf{T}}\kappa(t) &= \rho_{1i}, \\ \dot{\rho}_{(j+1)i} &= \rho_{(j+1)i}, \quad j = 1, \dots, m-1, \\ \dot{\rho}_{mi} &= 0, \end{aligned} \tag{26}$$

which coincides with (21).

From the nature of the system uncertainties and tail disturbances, the disturbance approximation error is absolutely bounded, that is, $|\tilde{\xi}_i(\cdot)| \le \xi_{i,\max} \in \mathbb{R}^+ < \infty$. Applying the control (23) in the ultra-local model (18) leads to the following tracking error dynamics:

$$\begin{aligned} e_{qi}^{(m+3)} + k_{(m+2)i}e_{qi}^{(m+2)} + \dots \\ + k_{(1)i}\dot{e}_{qi} + k_{(0)i}e_{qi} = \tilde{\xi}_i. \end{aligned} \tag{27}$$

By choosing the design control parameters such that the closed loop characteristic polynomial

$$s^{m+3} + k_{(m+2)i}s^{m+2} + \dots + k_{1(i)}s + k_{(0)i} \tag{28}$$

is Hurwitz (Ramírez-Neria *et al.*, 2014; 2016), the controller forces the tracking error to converge into a vicinity of the origin on the error phase plane, whose size is related to the gain control choice and the disturbance estimation error $\tilde{\xi}_i$. This can be proven using the following Lyapunov candidate function:

$$\begin{aligned} V_i(z) &= z_i^{\mathsf{T}} P_i z_i, \quad z_i \in \mathbb{R}^{m+3}, \\ P_i &= P_i^{\mathsf{T}} > 0, \quad P_i \in \mathbb{R}^{(m+3)\times(m+3)}, \\ z &= \begin{bmatrix} e_{qi} & \dot{e}_{qi} & \cdots & e_{qi}^{(m+2)} \end{bmatrix}. \end{aligned} \tag{29}$$

The state space realization of z_i is given by

$$\dot{z}_i = A_i z_i + b_i \xi_i \tag{30}$$

[1] Notice that this approximation is purely phenomenological, implying that the m-th time derivative of the ultra-local model is not a feature of the actual disturbance signal but a polynomial approximation. The disturbance approximation error term $\tilde{\xi}$ compensates for the approximate model scheme.

with

$$A_i = \begin{bmatrix} 0 & 1 & 0 & \cdots & 0 & 0 \\ 0 & 0 & 1 & \cdots & 0 & 0 \\ \vdots & \vdots & \vdots & \ddots & \vdots & \vdots \\ 0 & 0 & 0 & \cdots & 1 & 0 \\ 0 & 0 & 0 & \cdots & 0 & 1 \\ -k_{(0)i} & -k_{(1)i} & -k_{(2)i} & \cdots & -k_{(m+1)i} & -k_{(m+2)i} \end{bmatrix},$$

$$b_i = \begin{bmatrix} 0 & 0 & \cdots & 0 & 1 \end{bmatrix}^{\mathsf{T}}.$$

The time derivative of $V(z)$ is given by

$$\begin{aligned} \frac{\mathrm{d}V(z)}{\mathrm{d}t} &= 2z^{\mathsf{T}} P_i \dot{z} \\ &= z^{\mathsf{T}}(A_i^{\mathsf{T}} P_i + P_i A_i) z + 2z^{\mathsf{T}} P_i \tilde{\xi}_i. \end{aligned} \tag{31}$$

From the choice of (28) and the construction of A_i, A_i is Hurwitz. Then for any positive definite matrix P_i, there exists $Q_i = Q_i^{\mathsf{T}} > 0$, $Q_i \in \mathbb{R}^{(m+3)\times(m+3)}$ such that $A_i^{\mathsf{T}} P_i + P_i A_i = -Q_i$ (Sira-Ramírez *et al.*, 2017). The time derivative of $V(z)$ becomes

$$\frac{\mathrm{d}V(z)}{\mathrm{d}t} = -z^{\mathsf{T}} Q_i \dot{z} + 2z^{\mathsf{T}} P_i \tilde{\xi}_i. \tag{32}$$

Since $|\xi_i| \le \xi_{i,\max}$,

$$\begin{aligned} \frac{\mathrm{d}V(z)}{\mathrm{d}t} &\le -z^{\mathsf{T}} Q_i \dot{z} + 2\|z\|\|P_i\|\|\tilde{\xi}_i\| \\ &\le -z^{\mathsf{T}} Q_i \dot{z} + 2\xi_{i,\max}\|z\|\|P_i\|. \end{aligned} \tag{33}$$

Using the Rayleigh inequality in the last relation and simplifying, we get

$$\frac{\mathrm{d}V(z)}{\mathrm{d}t} \le \lambda_{\min}(Q_i)\|z\| \left[-\|z\| + 2\xi_{i,\max}\frac{\lambda_{\max}(P_i)}{\lambda_{\min}(Q_i)} \right]. \tag{34}$$

Thus, the time derivative of $V(z)$ is negative definite outside the set

$$\|z\| \le 2\xi_{i,\max}\frac{\lambda_{\max}(P_i)}{\lambda_{\min}(Q_i)},$$

forcing the tracking error vector z to be uniformly ultimately bounded, ensuring a ultimate bounded behaviour of the closed loop tracking error.

3.2.1. Flat filtering control synthesis as a compensation network. Transforming (23) into the Laplace domain, the compensation network representation of the controller is

$$\begin{aligned} &e_{vi}(s) \\ &= -\frac{k_{(m+1)i}s^{m+1} + \cdots + k_{(1)i}s + k_{(0)i}}{s^m(s + k_{(m+2)i})} e_{qi}(s). \end{aligned} \tag{35}$$

Defining $\eta_i := e_{qi}/s^m(s + k_{(m+2)i})$, the following representation in state variables is obtained:

$$\begin{aligned} \eta_{1i} &= \eta_i, \\ \dot{\eta}_{1i} &= \eta_{2i}, \\ &\vdots \\ \dot{\eta}_{mi} &= \eta_{m+1i}, \\ \dot{\eta}_{m+1i} &= -k_{(m+2)i}\eta_{m+1i} + e_{qi}. \end{aligned} \tag{36}$$

Finally, the time domain flat filter-based controller with m-th order ultra-local model approximation is

$$\begin{aligned} v_i = \ddot{q}_i^* &- k_{(m+1)}e_{qi} \\ &- (k_{(m+1)i}k_{(m+2)i} - k_{(m)i})\eta_{m+1i} \\ &- k_{(m-1)i}\eta_{mi} - \cdots - k_{(1)i}\eta_{2i} - k_{(0)i}\eta_{1i}, \\ &i = 1, 2. \end{aligned} \tag{37}$$

Furthermore, the closed-loop system with respect to the disturbance input results in a tracking error ruled by the attenuating features of the transfer function acting on the disturbance $\xi(s)_{qi}$ (Sira-Ramírez *et al.*, 2019)

$$\begin{aligned} &e_{qi}(s) \\ &= \frac{s^m(s + k_{(m+2)i})}{s^{m+3} + k_{(m+2)i}s^{m+2} + \cdots + k_{(1)i}s + k_{(0)i}} \\ &\quad \times \xi_{qi}(s). \end{aligned} \tag{38}$$

The last representation allows us to implement the controller as a compensation network. Besides, Eqn. (38) allows obtaining Bode's diagrams for disturbance attenuation analysis, which is important for periodic disturbances such as the possible arising ones for the TDFH system.

4. Numerical and experimental results

The detailed characterization of the system parameters is provided in Table 1.

The FFC and the well-known LQR control scheme were implemented for comparison purposes. The LQR gains were tuned through the optimization algorithm developed by Kumar *et al.* (2016). The used FFC consisted of two extended states; that is to say, the structure described in (23) with $m = 1$ was used.

Table 1. TDFH parameters.

Parameter	Variable	Value	Unit
Distance between RP and the rotation axis	rp	0.432	m
Distance between RC and the rotation axis	ry	0.233	m
Distance from the centre of mass on the rotation axis	L_{cm}	0.164	m
Helicopter body mass	m_h	1.03	kg
Moment of inertia in *pitch*	J_θ	0.09359	kg m^2
Moment of inertia in *yaw*	J_ψ	0.0947	kg m^2
Viscous friction in *pitch*	B_θ	0.01	Nms
Viscous friction in *yaw*	B_ψ	1	Nms
RP force constant over *pitch*	$k_{\theta\theta}$	0.7901	Nm/%pwm
RP force constant over *yaw*	$k_{\psi\theta}$	0.1426	Nm/%pwm
RC force constant over *yaw*	$k_{\psi\psi}$	-0.5078	Nm/%pwm
RC force constant over *pitch*	$k_{\theta\psi}$	0.0329	Nm/%pwm

This structure makes it possible to compensate for $\tilde{\xi}_i$ disturbances of the step and ramp type. Table 2 shows the poles used to tune the auxiliary controllers, proposed from the characteristic polynomial (28) describing the closed-loop error dynamics.

Now, the perturbation-driven closed-loop transfer function exhibits a large attenuation at both very low and high frequencies with a maximum amplitude at the bandwidth frequency (Sira-Ramírez *et al.*, 2019). Therefore, a Bode plot analysis of the perturbation-driven closed-loop transfer function introduces a high gain factor into the transfer function coefficients in terms of a small parameter ϵ, in the form

$$e_{qi}(s) = \left(\frac{s\left(s + \frac{k_{(3)i}}{\epsilon}\right)}{s^4 + \frac{k_{(3)i}}{\epsilon}s^3 + \frac{k_{(2)i}}{\epsilon}s^2 + \frac{k_{(1)i}}{\epsilon}s + \frac{k_{(0)i}}{\epsilon}} \right) \times \xi_{qi}(s). \tag{39}$$

with ϵ taking the values of $1,\ 0.5,\ 0.1,\ 0.05$ and 0.01. Figures 3(a) and (b) show the Bode diagrams for $i = 1, 2$, respectively. In both the cases it can be observed that the controllers generate disturbance attenuation at low and high frequencies. Furthermore, the use of high gain factors does not generate significant changes in the attenuation of disturbances.

On the other hand, the state feedback gains for the LQR were obtained using an optimization method developed by Kumar *et al.* (2016) which was used to control a TDFH. To perform the task, the system was linearized with the equilibrium point $\theta = 0,\ \dot{\theta},\ \psi = 0,\ \dot{\psi}$, while the matrices Q and R resulting from the optimization are

Table 2. Poles for the auxiliary controls.

γ	s_1	s_2	s_3	s_4
V_1	-43.28	-0.74	$-0.48 + 2.17i$	$-0.48 - 2.17i$
V_2	-5.01	-0.55	$-1.06 + 1.79i$	$-1.06 - 1.79i$

Table 3. Parameters of the Bézier polynomial.

γ^*	γ_i^*	γ_f^*	t_i	t_f
θ^*	-0.8 rad	0.2 rad	46 s	66 s
ψ^*	-0.3 rad	-0.3 rad	76 s	120 s

$$Q = \begin{bmatrix} 469.99 & 0 & 0 & 0 & 0 & 0 \\ 0 & 340.27 & 0 & 0 & 0 & 0 \\ 0 & 0 & 58.36 & 0 & 0 & 0 \\ 0 & 0 & 0 & 0.062 & 0 & 0 \\ 0 & 0 & 0 & 0 & 218.05 & 0 \\ 0 & 0 & 0 & 0 & 0 & 12.99 \end{bmatrix},$$

$$R = \begin{bmatrix} 12.99 & 0 \\ 0 & 476.69 \end{bmatrix}. \tag{40}$$

From the above, the resulting feedback gains K are

$$K = \begin{bmatrix} 0.95 & 0.219 & 0.62 & 0.025 & 0.9 & 0 \\ 2.9 & -9.19 & 1.412 & -0.9 & 1.1 & 0.5 \end{bmatrix}. \tag{41}$$

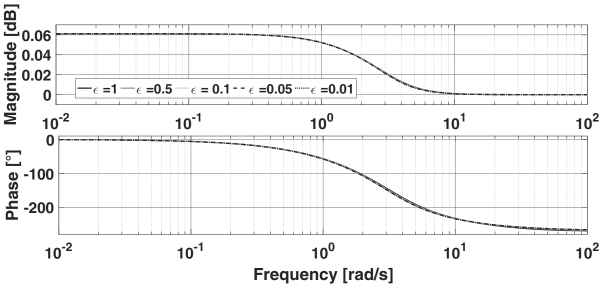

(a) $i = 1$

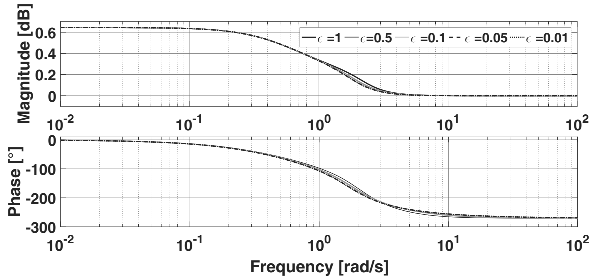

(b) $i = 2$

Fig. 3. Bode diagram of the closed-loop transfer function with disturbance input ξ for different values of the ϵ factor.

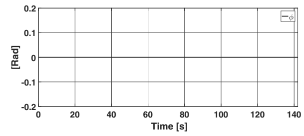

(a) Case 1.

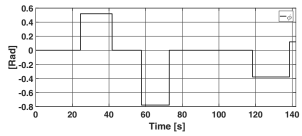

(b) Case 2.

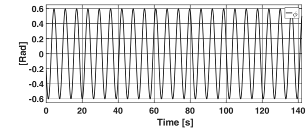

(c) Case 3.

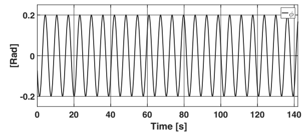

(d) Case 4.

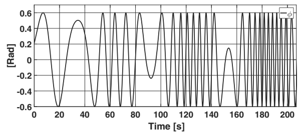

(e) Case 5.

Fig. 4. Disturbances (ϕ).

The desired trajectories were Bézier polynomials, for which the parameters of initial position γ_i^*, final position γ_f^*, initial time t_i and final time t_f are described in Table 3. Initially, the system is at rest, then the initial position in pitch is 0.9 [rad], the position of yaw is 0 rad and its speed is 0 rad/s. Moreover, the sampling frequency is 1 KHz.

In addition, both control schemes were assessed in five different cases related to the applied disturbances (ϕ) in TR, illustrated by Fig. 4. In one hand, for the first case the disturbance in ϕ is zero, so there is no disturbance in TR. On the other hand, Case 2 presents a series of step-type disturbances in ϕ of different values, alternating the incidence in TR on the rotation axes. Cases 3 and 4 include sinusoidal disturbances in ϕ, which have an amplitude of 0.6 and 0.2 [rad] respectively with a frequency of 1 [rad/s]; Cases 3 and 4 contain the same frequency but different amplitudes to validate that the FFC control scheme can attenuate periodic disturbances. These disturbances generate a regular variation in the incidence and TR on the rotation axes. On the other hand, Case 5 is sinusoidal with a variable frequency of the form $0.6\sin((t+6)\sin(0.05(t+6))0.2)$ which allows submitting to the system under irregularities in the incidence and TR on the rotation axes.

4.1. Simulation and experimental results. The simulation results of both the control schemes are presented in Figs. 5 and 6, where the dynamics in pitch exposed to the five disturbance cases is presented in Fig. 5

Table 4. Integral of the simulated squared error.

	FFC		LQR	
Case	ISE$_\theta$	ISE$_\psi$	ISE$_\theta$	ISE$_\psi$
Case 1	0.004	0.036	0.14	0.045
Case 2	0.066	0.039	0.244	0.075
Case 3	0.848	0.115	5.319	0.545
Case 4	0.081	0.037	0.61	0.089
Case 5	0.887	0.118	6.362	0.709

and the dynamics in yaw is shown in Fig. 6. In these figures, it can be verified that the four disturbance cases affect both coordinates and, apart from this, both schemes are capable of tracking the desired trajectories. However, there is a larger attenuation of the disturbances by the FFC. In addition, Table 4 shows the integral of the squared error (ISE) for each control scheme with respect to each coordinate, where it can be verified that the FFC scheme has better performance against the LQR by having a lower magnitude of the ISE for each case. Therefore, Case 5 generates more effort for the control schemes since it generates the highest ISE values.

4.2. Experimental results. Figure 7 shows the pitch angle (θ) in response to the five disturbance cases. Notice that both control schemes manage to stabilize the pitch angle trying to follow the reference trajectory and compensate the disturbances as well. In addition, it is evident that the pitch response of the LQR presents a faster response time; however, this results in a larger overshoot in the first seconds of path tracking and, in turn, larger

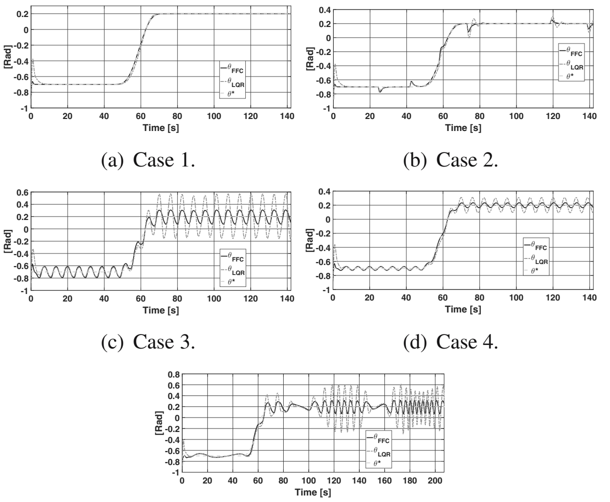

(a) Case 1. (b) Case 2. (c) Case 3. (d) Case 4. (e) Case 5.

Fig. 5. Simulation results for the pitch angle (θ).

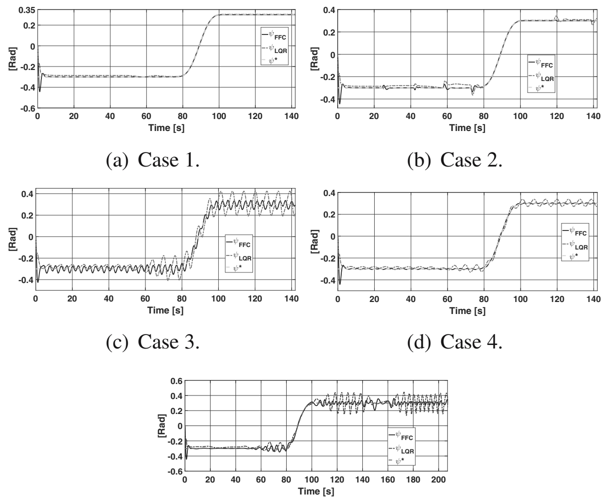

(a) Case 1. (b) Case 2. (c) Case 3. (d) Case 4. (e) Case 5.

Fig. 6. Simulation results for the yaw angle (ψ).

oscillations around the desired path compared with the response of the FFC control.

Likewise, when comparing the unperturbed TR case of Fig. 7(a) with Fig. 7(b) of Case 2, a similar behaviour can be observed between both the cases for each control scheme, both the schemes being capable of compensating the disturbances of Fig. 4(b). However, the FFC has better performance than the LQR as it has smaller amplitude oscillations.

Besides, Figs. 7(c) and (d) of Cases 3 and 4 respectively, also show a similar behaviour to that of the unperturbed case of Fig. 7(a); Figs. 7(c) and (d) show oscillations on the desired path with a similar frequency to the disturbance in TR. In addition, Case 3, having a larger amplitude in the disturbance in TR, generates a larger oscillation in the pitch angle, unlike Case 4. On the other hand, the pitch response to Case 5 (Fig. 7(e)) shows the FFC scheme exhibits a similar response to Case 3; thus, the scheme can attenuate the disturbance, achieving robustness to the frequency of the disturbance. However, the LQR generates larger oscillations around the trajectory compared with the previous cases. Also, like the previous cases, the FFC yields a better tracking performance with respect to the LQR.

In the same manner, the behaviour in yaw (ψ) in the four test cases can be observed in Fig. 8(e), where the control schemes are also capable of stabilizing the axis of rotation trying to follow the trajectory. However, the LQR control presents instability after 120 s presumably generated by the disturbance in ϕ of Case 2. In the same way, in Case 5, the yaw stability is lost after 80 s, which is the moment in which the Bezier polynomial starts and perturbation of ϕ reaches a higher frequency. Furthermore, using the FFC the yaw behaviour is quite similar in all five cases; therefore, the control scheme manages to compensate the disturbances that arise in TR.

Also, the yaw response of the LQR control is more aggressive at the beginning of the follow-up; this generates a larger effort in the controller to achieve stability since, in both the cases, it starts with a desired position of the step type.

On the other hand, Fig. 9(e) shows the control actions U_θ and U_ψ of both the control schemes in the four cases; the these control actions are given in percentage of PWM. It is worth mentioning that the rotor drivers are configured in a PWM percentage range of 4 to 10 units at a frequency of 50 Hz, so that the values shown in the graphs of Fig. 9(e) are such that the zero value of the controller configuration has to be included. That is, the PWM signal emitted to the controllers turns out to be $U_\theta + 4$ or, likewise, $U_\psi + 4$.

Finally, Table 5 shows the value of the integral of the squared error of pitch (ISE$_\theta$), yaw (ISE$_\psi$) and their sum (ISE$_{\theta+\psi}$) for each case. In this manner, it is possible to corroborate the performance of the control schemes on each global y coordinate, where in each case the FFC generates lower ISE values compared with the LQR, so that the flat filtering shows a higher overall tracking performance compared with the LQR. In addition, Fig. 10 shows the evolution of the global squared error integral of each control scheme of Case 1 (top panel) and Case 5 (bottom panel).

5. Conclusions

The obtained mathematical model describes the TDFH dynamics regarding any type of disturbance in TR. In this way, the analysis and prediction of the behaviour of its rotation axes in the presence of disturbances can be carried

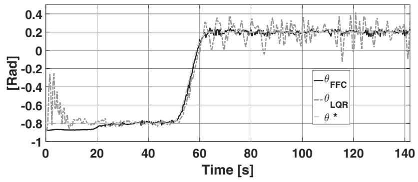

(a) Case 1.

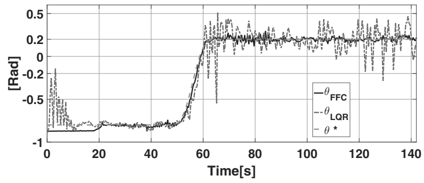

(b) Case 2.

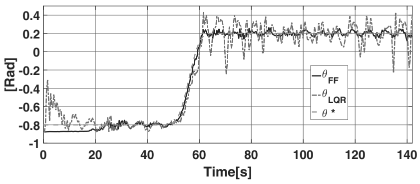

(c) Case 3.

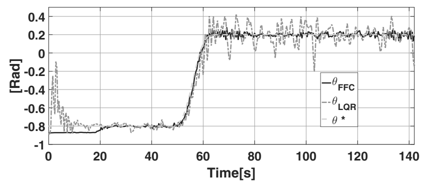

(d) Case 4.

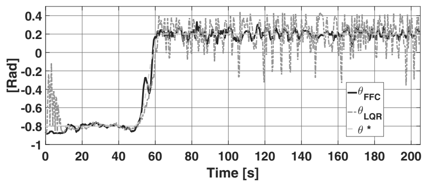

(e) Case 5.

Fig. 7. Experimental results for the pitch angle (θ).

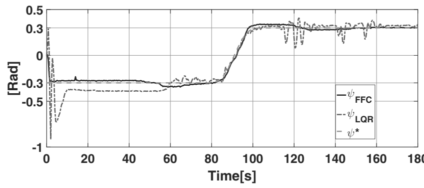

(a) Case 1.

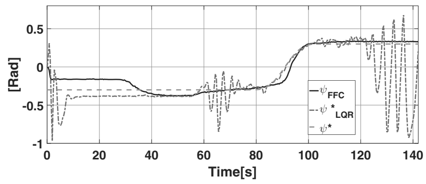

(b) Case 2.

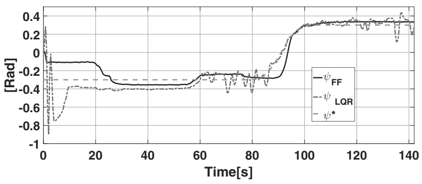

(c) Case 3.

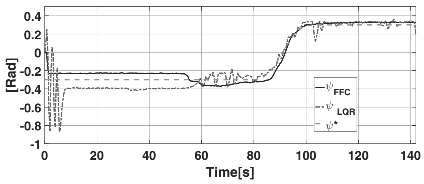

(d) Case 4.

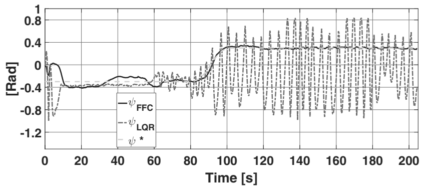

(e) Case 5.

Fig. 8. Experimental results for the yaw angle (ψ).

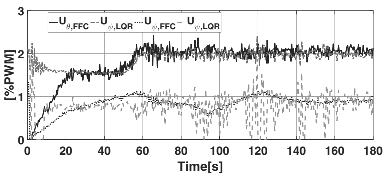

(a) Case 1.

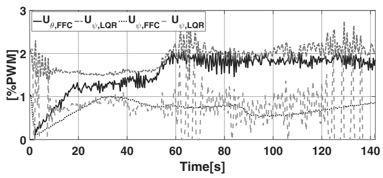

(b) Case 2.

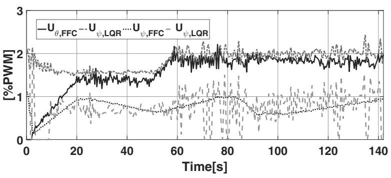

(c) Case 3.

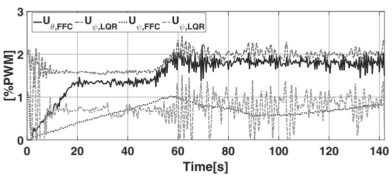

(d) Case 4.

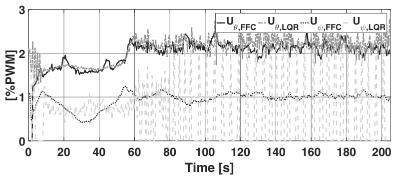

(e) Case 5.

Fig. 9. Control action (U).

Table 5. Integral of the squared error (ISE).

Case	FFC			LQR		
	ISE_θ	ISE_ψ	$\mathrm{ISE}_{(\theta+\psi)}$	ISE_θ	ISE_ψ	$\mathrm{ISE}_{(\theta+\psi)}$
Case 1	0.48	0.51	0.98	3.67	3.93	7.6
Case 2	0.49	2.34	2.84	6.83	26.15	32.98
Case 3	0.52	3.3	3.82	4.68	4.9	9.58
Case 4	0.45	1.28	1.74	4.46	4.05	8.82
Case 5	1.21	2.71	3.93	12.02	124.34	136.36

out in a controlled manner in ϕ. Furthermore, this model converges to the one reported in the literature for the case when the disturbance ϕ is zero.

The simulation results show that both the control schemes manage to stabilize the system although they present oscillations around the trajectory in Cases 3, 4 and 5, where the FFC yields better robustness by having lower magnitude of oscillations caused by the disturbances and presenting lower accumulated magnitude of the ISE than the LQR scheme.

Concerning the tracking results, the FFC has better performance compared with the LQR control, as it yields smaller values in the ISE for all the reported tests. In addition, from Table 5 it can be observed that the values of the ISE of the FFC are quite similar, which is an indicator that this control scheme has higher robustness with respect to the popular LQR control.

Accordingly, step type disturbances in TR when varying ϕ can be compensated by the FFC by stabilizing and following the trajectory in both the axes. In addition, tracking control tasks can be executed in the case of sinusoidal disturbances. However, these perturbations maintain oscillations around the desired path with the same frequency as the ϕ perturbations in the pitch behaviour. The control scheme achieves yaw stabilization and tracking, compensating for the periodic sinusoidal perturbations unlike those originating in TR.

Moreover, it can be seen that the amplitude of the pitch oscillations around the desired trajectory is related to the amplitude of the disturbances in ϕ, since in Cases 3 and 5, these oscillations are displayed with a larger amplitude where the sinusoidal perturbation amplitude is 0.6 rad unlike Case 4 where the perturbation amplitude is 0.2 rad.

In addition, it is possible to observe that the behaviour of the simulated and experimental results of the FFC scheme are similar, especially in Cases 3, 4 and 5, maintaining the oscillations around the trajectory with the same frequency and amplitude ratio of the disturbances. On the other hand, contrary to what is presented in simulation, the LQR scheme presents complications in stability in Cases 2 and 5. This may be due to non-modelled dynamics of the TDFH. These comparisons show that the FFC is more robust against generated disturbances and non-modelled dynamics.

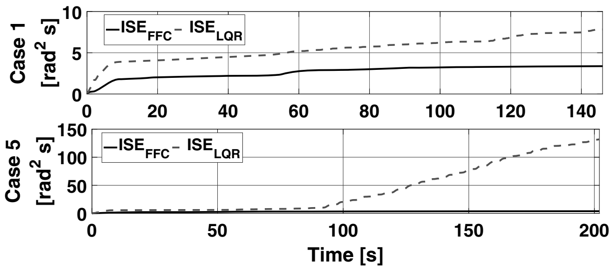

Fig. 10. Evolution of the integral of the squared error.

The proposed FFC scheme showed relevant results for rejecting of disturbances that frequently affect the TR, which usually cause stability problems during the flight and limit the manoeuvring space (Sánchez-Meza *et al.*, 2020). These perturbations include aerodynamic interference between the MR and the TR (Fletcher and Brown, 2008), aerodynamic forces, and the tail shake phenomenon (Schäferlein *et al.*, 2018), among others.

In addition, the disturbance analyzed usually occurs in hybrid UAVs, e.g., the tiltrotor-type aircraft, where its inertia tensor and dynamic parameters change depending on the inclination of the nacelle (Cerezo-Pacheco *et al.*, 2021). Adjusting the tilt angle of the rotor causes significant changes in the aircraft's structural and mechanical properties, directly affecting its stability. Thus, our proposal could be modified to incorporate this type of vehicle, where the transition stage from one flight mode to another is usually the most critical (Ta *et al.*, 2012).

Acknowledgment

This article was partially supported by Secretaría de Investigación y Posgrado, Instituto Politécnico Nacional, under the grants 20232388, 20231585, 20231632 and 20230569. Victor G. Sánchez-Meza is a scholarship holder of CONACYT (964590).

References

Ahi, B. and Haeri, M. (2018). Linear active disturbance rejection control from the practical aspects, *IEEE/ASME Transactions on Mechatronics* **23**(6): 2909–2919.

Ahmed, Q., Bhatti, A., Iqbal, S. and Kazmi, I. (2010). 2-Sliding mode based robust control for 2-DOF helicopter, *11th International Workshop on Variable Structure Systems (VSS), Mexico City, Mexico*, pp. 481–486.

Bortoff, S.A. (1999). The University of Toronto RC helicopter: A test bed for nonlinear control, *Proceedings of the 1999 IEEE International Conference on Control Applications, Kohala Coast, USA*, Vol. 1, pp. 333–338.

Budiyono, A. and Wibowo, S. (2007). Optimal tracking controller design for a small scale helicopter, *Journal of Bionic Engineering* **4**(4): 271–280.

Butt, S.S. and Aschemann, H. (2015). Multi-variable integral sliding mode control of a two degrees of freedom helicopter, *IFAC-PapersOnLine* **48**(1): 802–807.

Cerezo-Pacheco, A.D., Pérez-Velasco, C.A., Lozano-Hernandez, Y., Rodriguez-Cortes, H. and Sánchez-Meza, V.G. (2021). Integration of x-plane and Matlab for modeling and simulation of a tiltrotor UAV, *2021 International Conference on Mechatronics, Electronics and Automotive Engineering (ICMEAE), Cuernavaca, Mexico*, pp. 39–44.

Fareh, R., Khadraoui, S., Abdallah, M.Y., Baziyad, M. and Bettayeb, M. (2021). Active disturbance rejection control for robotic systems: A review, *Mechatronics* **80**: 102671.

Ferdaus, M.M., Anavatti, S.G., Pratama, M. and Garratt, M.A. (2020). Towards the use of fuzzy logic systems in rotary wing unmanned aerial vehicle: A review, *Artificial Intelligence Review* **53**(1): 257–290.

Fletcher, T.M. and Brown, R.E. (2008). Main rotor-tail rotor interaction and its implications for helicopter directional control, *Journal of the American Helicopter Society* **53**(2): 125–138.

Fliess, M. and Join, C. (2013). Model-free control, *International Journal of Control* **86**(12): 2228–2252.

Fliess, M., Lévine, J., Martin, P. and Rouchon, P. (1995). Flatness and defect of non-linear systems: Introductory theory and examples, *International Journal of Control* **61**(6): 1327–1361.

Fliess, M., Marquez, R., Delaleau, E. and Sira-Ramirez, H. (2002). Correcteurs proportionnels-intégraux généralisés, *ESAIM: Control, Optimisation and Calculus of Variations* **7**: 23–41.

Garcia, R. and Valavanis, K.P. (2008). The implementation of an autonomous helicopter testbed, *in* P. Valavanis *et al.* (Eds), *Unmanned Aircraft Systems*, Springer, Dordrecht, pp. 423–454.

Han, J. (2009). From PiD to active disturbance rejection control, *IEEE Transactions on Industrial Electronics* **56**(3): 900–906.

He, M., He, J. and Scherer, S. (2021). Model-based real-time robust controller for a small helicopter, *Mechanical Systems and Signal Processing* **146**: 1–16, Article no. 107022.

Kantue, P. and Pedro, J.O. (2022). Integrated fault-tolerant control of a quadcopter UAV with incipient actuator faults, *International Journal of Applied Mathematics and Computer Science* **32**(4): 601–617, DOI: 10.34768/amcs-2022-0042.

Kasac, J., Kotarski, D. and Piljek, P. (2019). Frequency-shifting-based algebraic approach to stable on-line parameter identification and state estimation of multirotor UAV, *Asian Journal of Control* **21**(4): 1619–1629.

Kumar, E.V., Raaja, G.S. and Jerome, J. (2016). Adaptive PSO for optimal LQR tracking control of 2 DOF laboratory helicopter, *Applied Soft Computing* **41**: 77–90.

Kutay, A.T., Calise, A.J., Idan, M. and Hovakimyan, N. (2005). Experimental results on adaptive output feedback control using a laboratory model helicopter, *IEEE Transactions on Control Systems Technology* **13**(2): 196–202.

Leishman, J.G. (2007). *The Helicopter*, College Park Press, College Park, MD.

Liu, C. (2022). Stabilization control of quadrotor helicopter through matching solution by controlled Lagrangian method, *Asian Journal of Control* **24**(4): 1885–1894.

Lozano-Hernandez, Y. and Gutierrez-Frias, O. (2016). Design and control of a four-rotary-wing aircraft, *IEEE Latin America Transactions* **14**(11): 4433–4438.

Lynn, R.R., Robinson, F., Batra, N. and Duhon, J. (1970). Tail rotor design. Part I: Aerodynamics, *Journal of the American Helicopter Society* **15**(4): 2–15.

Madoński, R. and Herman, P. (2015). Survey on methods of increasing the efficiency of extended state disturbance observers, *ISA Transactions* **56**: 18–27.

Nilsen, S. (2017). *Modelling and Control of Two Degrees of Freedom Helicopter Model*, MS thesis, Høgskolen i Sørøst-Norge, Notodden.

Nonami, K., Kendoul, F., Suzuki, S., Wang, W. and Nakazawa, D. (2010). *Autonomous Flying Robots: Unmanned Aerial Vehicles and Micro Aerial Vehicles*, Springer, Tokyo.

Ordaz, P., Alazki, H., Sánchez, B. and Ordaz-Oliver, M. (2023). On the finite time stabilization via robust control for uncertain disturbed systems, *International Journal of Applied Mathematics and Computer Science* **33**(1): 71–82, DOI: 10.34768/amcs-2023-0006.

Pereira das Neves, G. and Augusto Angélico, B. (2022). Model-free control of mechatronic systems based on algebraic estimation, *Asian Journal of Control* **24**(4): 1575–1584.

Pizetta, I.H.B., Brandao, A.S. and Sarcinelli-Filho, M. (2016). A hardware-in-the-loop platform for rotary-wing unmanned aerial vehicles, *Journal of Intelligent & Robotic Systems* **84**(1): 725–743.

Raffo, G.V., Ortega, M.G. and Rubio, F.R. (2015). Robust nonlinear control for path tracking of a quad-rotor helicopter, *Asian Journal of Control* **17**(1): 142–156.

Ramírez-Neria, M., Gao, Z., Sira-Ramirez, H., Garrido-Moctezuma, R. and Luviano-Juarez, A. (2021). On the tracking of fast trajectories of a 3 DOF torsional plant: A flatness based ADRC approach, *Asian Journal of Control* **23**(3): 1367–1379.

Ramírez-Neria, M., Sira-Ramírez, H., Garrido-Moctezuma, R. and Luviano-Juarez, A. (2014). Linear active disturbance rejection control of underactuated systems: The case of the furuta pendulum, *ISA Transactions* **53**(4): 920–928.

Ramírez-Neria, M., Sira-Ramírez, H., Garrido-Moctezuma, R. and Luviano-Juárez, A. (2016). On the linear control of underactuated nonlinear systems via tangent flatness and active disturbance rejection control: The case of the ball and beam system, *Journal of Dynamic Systems, Measurement, and Control* **138**(10): 104501.

Rojas-Cubides, H., Cortés-Romero, J., Coral-Enriquez, H. and Rojas-Cubides, H. (2019). Sliding mode control assisted by GPI observers for tracking tasks of a nonlinear multivariable twin-rotor aerodynamical system, *Control Engineering Practice* **88**: 1–15.

Ross, J., Seto, M. and Johnston, C. (2022). Autonomous landing of rotary wing unmanned aerial vehicles on underway ships in a sea state, *Journal of Intelligent & Robotic Systems* **104**(1): 1–9.

Rysdyk, R.T. and Calise, A.J. (1999). Adaptive model inversion flight control for tilt-rotor aircraft, *Journal of Guidance, Control, and Dynamics* **22**(3): 402–407.

Sánchez-Meza, V. G., Lozano-Hernández, Y. and Gutiérrez-Frías, O.O. (2020). Modeling and control of a two DOF helicopter with tail rotor disturbances, *International Conference on Mechatronics, Electronics and Automotive Engineering (ICMEAE)*, pp. 79–84.

Schäferlein, U., Keßler, M. and Krämer, E. (2018). Aeroelastic simulation of the tail shake phenomenon, *Journal of the American Helicopter Society* **63**(3): 1–17.

Siciliano, B., Sciavicco, L., Villani, L. and Oriolo, G. (2010). *Robotics: Modelling, Planning and Control*, London.

Sira-Ramírez, H. (2018). From flatness, GPI observers, GPI control and flat filters to observer-based ADRC, *Control Theory and Technology* **16**(4): 249–260.

Sira-Ramírez, H., Luviano-Juárez, A., Ramírez-Neria, M. and Zurita-Bustamante, E.W. (2017). *Active Disturbance Rejection Control of Dynamic Systems: A Flatness Based Approach*, Butterworth-Heinemann, Kidlington.

Sira-Ramírez, H., Zurita-Bustamante, E.W. and Huang, C. (2019). Equivalence among flat filters, dirty derivative-based PID controllers, ADRC, and integral reconstructor-based sliding mode control, *IEEE Transactions on Control Systems Technology* **28**(5): 1696–1710.

Spong, M., Hutchinson, S. and Vidyasagar, M. (2006). *Robot Modeling and Control*, Wiley, Hoboken.

Ta, D.A., Fantoni, I. and Lozano, R. (2012). Modeling and control of a tilt tri-rotor airplane, *2012 American Control Conference (ACC), Montreal, Canada*, pp. 131–136.

Tang, P., Wang, F. and Dai, Y. (2019). Controller design for different electric tail rotor operating modes in helicopters, *International Journal of Pattern Recognition and Artificial Intelligence* **33**(08): 1959022.

Tanner, O. and Geering, H.P. (2003). Two-degree-of-freedom robust controller for an autonomous helicopter, *Proceedings of the American Control Conference, Denver, USA*, Vol. 2, pp. 993–998.

Tavoosi, J. (2021). Hybrid intelligent adaptive controller for tiltrotor UAV, *International Journal of Intelligent Unmanned Systems* **9**(4): 256–273.

Velagic, J. and Osmic, N. (2010). Design and implementation of fuzzy logic controllers for helicopter elevation and azimuth controls, *Conference on Control and Fault-Tolerant Systems (SysTol), Nice, France*, pp. 311–316.

Vitzilaios, N.I. and Tsourveloudis, N.C. (2009). An experimental test bed for small unmanned helicopters, *Journal of Intelligent and Robotic Systems* **54**(5): 769–794.

Wang, B., Shen, Y. and Zhang, Y. (2020). Active fault-tolerant control for a quadrotor helicopter against actuator faults and model uncertainties, *Aerospace Science and Technology* **99**: 105745.

Zeng, Y., Xu, J. and Zhang, R. (2019). Energy minimization for wireless communication with rotary-wing UAV, *IEEE Transactions on Wireless Communications* **18**(4): 2329–2345.

Zhan, C. and Huang, R. (2020). Energy efficient adaptive video streaming with rotary-wing UAV, *IEEE Transactions on Vehicular Technology* **69**(7): 8040–8044.

Zhu, B. and Huo, W. (2013). Robust nonlinear control for a model-scaled helicopter with parameter uncertainties, *Nonlinear Dynamics* **73**(1): 1139–1154.

Victor G. Sánchez-Meza is a control and automation engineer, who graduated from ESIME-IPN, Mexico, in 2018, and obtained his MS degree in advanced technology at UPIITA-IPN in 2021. He is presently working towards a PhD in advanced technology there. His current research interests include dynamic systems control, UAV control, robotic systems, and mechatronics.

Yair Lozano-Hernández was born in Hidalgo, Mexico. He received his BS degree in control and automation in 2013 at the School of Electrical and Mechanical Engineering of the National Polytechnic Institute (ESIME-IPN), and his MSc and PhD degrees from the Professional School of Engineering and Advanced Technologies of the National Polytechnic Institute of Mexico (UPIITA-IPN) in 2016 and 2019, respectively. He is currently a researcher at the Interdisciplinary Professional Unit of Engineering, Campus Hidalgo (UPIIH), of the IPN. His research interests are automatic control, design control systems for UAV, control of nonlinear systems, and underactuated systems.

Oscar Octavio Gutiérrez Frías was born in Mexico City. He received his BS degree in mechatronics from the Professional School of Engineering and Advanced Technologies of the National Polytechnic Institute of Mexico (UPIITA-IPN) in 2003. He obtained an MSc degree in computing engineering from the Computing Research Center of the National Polytechnic Institute in 2006. In 2009, he received a PhD in computer science at CIC-IPN. Since 2012, he has been with the Graduate Section at UPIITA-IPN. His research focuses on non-linear systems control, underactuated systems, robotics, and automation

Norma Lozada-Castillo holds a BS degree from the Superior School of Physics and Mathematics, as well as MS and PhD degrees from CINVESTAV, Automatic Control Department, National Polytechnic Institute. Her research interests include stochastic control, nonlinear control, and estimation in stochastic systems.

Alberto Luviano-Juárez received his BS degree in mechatronics at Instituto Politécnico Nacional (IPN) in 2003, his MSc degree in automatic control and his PhD degree from Centro de Investigación y de Estudios Avanzados (CINVESTAV), Mexico, in 2006 and 2011, respectively. Since 2011, he has been with the Graduate Section at UPIITA-IPN. His research interests include robotic systems, and estimation and control of mechatronic systems.

Received: 2 October 2022
Revised: 21 February 2023
Re-revised: 17 May 2023
Accepted: 22 May 2023